Fracture processes imaging in concrete using nonlinear ultrasound

Martin Lott, Marcel C Remillieux, Vincent Garnier, T.J. J Ulrich, Pierre-Yves Le Bas, Arnaud Deraemaeker, Cédric Dumoulin, Cédric Payan

Fracture processes imaging in concrete using nonlinear ultrasound

Martin Lott[1,2], Marcel C. Remillieux[3], Vincent Garnier[2], T. J. Ulrich[4], Pierre-Yves Le Bas[4], Arnaud Deraemaeker[5], Cédric Dumoulin[5], Cédric Payan[2]

[1]Université Grenoble Alpes, Université Savoie Mont Blanc, CNRS, IRD, IFSTTAR, ISTerre, 38000 Grenoble, France

[2]Aix Marseille Univ, CNRS, Centrale Marseille, LMA, Marseille, France

[3]Geophysics Group (EES-17), Los Alamos National Laboratory, Los Alamos, NM, 87545, USA

[4]Detonation Science and Technology Group (Q-6), Los Alamos National Laboratory, Los Alamos, NM, 87545, USA

[5]Université Libre de Bruxelles, BATir Department, F. D. Roosevelt Av 50, 1050 Brussels, Belgium

Abstract

This paper shows the complementarity of two nonlinear ultrasonic imaging methods to characterize closed macro cracks in concrete. A time reversal mirror is used to locally probe and image the nonlinearity of a cracked region. Two nonlinear parameters are extracted to map the cracked region. The image obtained using the first parameter relates the harmonic generation due to the contact and frictional behaviors at the crack lips, correlated with vibro-thermography imaging of the same crack. The image obtained using the second parameter is based on the conditioning of the material induced by distributed micro cracks arising from the fracture process zone. These results show a great potential for characterization of fracture processes in concrete, with the possibility to uncouple the effects of the crack itself from surrounding distributed micro damage.

Keywords: Nonlinear ultrasound, Concrete, Cracks, Fracture process zone

Highlight:

- Nonlinear ultrasound can image and distinguish fracture processes in concrete
- Nonlinear responses from the fracture process zone and the crack lips are separated
- The results are correlated with vibro-thermography images

1. Introduction

In civil engineering, increasingly more stringent safety and maintenance requirements have called for more sophisticated detection and imaging NDT tools. This is particularly true in the nuclear-energy industry, in the context of license renewal and need for structural assessment. Ultrasonic assessment of concrete structures has been successfully achieved since 1990's with the possibility to image complex structures using tomographic approaches [1,2]. Ultrasonic crack-depth estimation in concrete is standardized [3], based on low-frequency (tens of kHz) wave propagation. However, the resolution is limited by the wavelength and only the opened portion of the crack can be detected. More refined methods based on the multiple scattering of higher-frequency waves [4] are more sensitive to the complex morphology of the crack, including partially opened cracks [5]. Nonlinear-ultrasonic-based methods have been proven efficient in detecting many types of damage and pathologies in concrete [6,7,8,9]. Nonlinear ultrasound has also been successfully employed to probe closed cracks [10,11] and exhibited a promising sensitivity. Even if the industrial civil engineering community reveals a growing interest for these methods, nonlinear ultrasonic inspection of concrete has been limited to laboratory studies.

So far, ultrasonic imaging of closed cracks remains a challenge. As for characterization, ultrasonic imaging can be achieved [12] but with a sensitivity limited to the large wavelength employed and to the opened portion of the crack. Again, higher frequencies fall in the multiple scattering regime into which standard methods do not apply. Recent research based on higher frequency diffuse waves showed the ability to image macro crack in laboratory samples [13] as well as real structures [14]. However, this approach only applies to image variations, i.e., crack propagation or crack opening due to external loadings, and only image the opened portions of the cracks.

The aim of this paper is to investigate the potential of methods based on nonlinear acoustics for closed-crack imaging. The imaging method employed here is based on time reversal, which focuses elastic energy at a prescribed location [15]. A study of the amplitude dependence of the elastic response allows then to locally probe the nonlinearity of the medium. Repeating this experiment over a regular grid spanning a region of interest on the surface of the concrete may provide a map of the nonlinearity. Such a method was already applied to probe distributed damage in concrete [16], as well as in other materials

55 such as metals [17]. This paper shows that contact phenomena at the crack lips are well imaged using a

56 method based on harmonic generation. These physical phenomena are also validated using active vibro-

57 thermography. The fracture process zone surrounding the main crack lips exhibits micro damage

58 occurring during fracture formation [18]. This zone is also imaged using a time-delay method, similar

59 to the one used in [16].

60

61 **2. Materials and Methods**

62 We study a notched rectangular prism of ordinary concrete with dimensions of $10 \times 10 \times 60$ cm^3. The

63 composition of the sample is provided in table.1.

64 Table.1. Concrete sample composition

CEM I 52.5 N PMES CP2 (Saint Vigor, FR)	340 kg/m^3
Sand 0/4 (Bernières, FR)	739 kg/m^3
Gravel 8/22 (Bernières, FR)	1072 kg/m^3
Total water	184 kg/m^3

65

66 A macro-crack departing from the notch was generated in the sample via a three-point bending test.

67 Photographs of the sample and crack are shown in Figure 1(a,c) as well as the force versus vertical

68 displacement curve recorded during the mechanical test (Fig.1b).

69 In the following, our ultrasonic measurements capitalize on a well-known property of elastic waves to

70 focus a high level of elastic energy in time and space, namely a Time Reversal Mirror (TRM). A

71 description of time reversal and its application to non-destructive testing was given by Anderson et al.

72 [19]. The reciprocal TRM version employed in this study provides an opportunity to focus energy

73 remotely from a set of source transducers. After the forward step has been conducted independently with

74 each of these source transducers, they can be synchronized to emit simultaneously their TR signals and

75 focus elastic wave energy at a point of interest, thus allowing relatively large strain amplitudes to be

76 reached. The large strain amplitude is necessary for the study of nonlinearity while the localized

77 excitation is necessary for imaging application, to probe the nonlinearity of the material locally (e.g.,

78 near a crack).

79   The sample was instrumented with 10 piezoelectric disks, which were used as source transducers

80   randomly glued on the six faces of the sample. The piezoelectric disks were made by APC International

81   using material type 855 (Navy VI), had a diameter of 25.4 mm and thickness of 6.3mm. Devcon® 5

82   Minute epoxy was used to bond the transducers to the concrete sample. The source transducers were

83   individually driven with signals generated by 16-bit waveform-generator cards (National Instrument,

84   PXI-5421) and amplified 50 times by power amplifiers (Tabor Electronics, Model 9400). The out-of-

85   plane component of the particle velocity was measured on the surface of the sample using a laser Doppler

86   vibrometer (Polytec OFV-303). The laser head was mounted on a moving stage capable of scanning the

87   vibration field on a region of interest. The data measured by this instrument was digitized at a sampling

88   rate of 10 MHz (National Instrument, PXI-4122) with a sensitivity of 5 mm/s/V. The linearity of the

89   setup was checked on a plexiglass sample.

90   In this experiment, the band-limited impulse response between the sources and the receiver (focal point)

91   are obtained using a combination of chirp signals and cross-correlations, to increase the signal-to-noise

92   ratio in the frequency band of interest. The chirp signal used in the forward step had a frequency range

93   of 50 kHz to 150 kHz, which encompasses the operating frequency of the piezoelectric source at 80

94   kHz. The full TRM procedure used in this study is gathered in Figure 2. Figure 2a shows the ten forward

95   signals (band-limited impulse responses) obtained independently for the ten source transducers by cross-

96   correlation with the laser signal at the focal point. Once reversed in time, the summation of the ten

97   sources give rises to a localized signal in time (Fig 2b) and space (Fig 2c). In Figure 2c, the white cross

98   denotes the point in space where the ten signals in Figure 2a and the time reversed summation is

99   recorded. Theoretically, the full-width half-maximum (FWHM) size of a focal spot is equal to a half

100   wavelength at the center frequency of the pulse [20]. As shown in Figure 2c, the size of the measured

101   focal spot is approximately 1 cm. Considering a center frequency of 100 kHz, we estimate the wave

102   speed to be approximately 2000 m/s, which would correspond to the wave speed of surface waves in

103   concrete [21]. In other words, the focal signal in this particular setup is mainly produced by surface

104   waves. The *local* (at the focal spot) strain amplitude is approximated as the ratio between the out-of-

105   plane particle velocity and the mean wave speed as in [16]. This estimation of the strain amplitude is

106   essential for quantitative nonlinear studies [16,22].

107   TR-based imaging was performed around the crack and above the notch, within a square region of $60 \times$

108   60 mm^2. The scan grid consisted of 1600 points with a spatial resolution of 1.5 mm. At each scan point,

109   the TR experiment was repeated at 10 amplitudes (before amplification): 5 negative amplitudes $x_i^- = $ -

110   1V, -0.8V, -0.6V, -0.4V, -0.2V, and 5 positive amplitudes $x_i^+ = 0.2\text{V}, 0.4\text{V}, 0.6\text{V}, 0.8\text{V}, 1\text{V}$. The phase

111   shift in the amplitude sweep will be useful in the nonlinear analysis. The TR signals obtained at a point

112   of focus on the scanning grid with the 10 source amplitudes are shown in Figure 2a. Two nonlinear

113   parameters are extracted from this set of data: one that is representative of a diffuse damage of the

114   sample [16] and one that is representative of clapping phenomena at the crack lips interface [7,17].

115

116   The first parameter is related to the time at which the maximum signal amplitude is achieved at the focal

117   point, which we will refer to as focal time. The signals shown in Figure 3a-1 are used for this analysis.

118   The dependence of the focal time on the vibration amplitude is related to nonclassical nonlinearity and

119   will be described by a parameter α [16]. The focal time at the lowest vibration amplitude of the

120   experiment is used as a linear reference against which the focal times at the larger vibration amplitudes

121   are compared to compute a time delay using cross correlation. The time delay experienced by the focal

122   signal as a function of strain amplitude at this particular focal point is shown in Fig. 3a-2 for the 5

123   positive source amplitudes (from 0.2V to 1V). The slope of the linear fit for this set of time delays is the

124   parameter α used in this analysis.

125

126   The second parameter is estimated using the pulse inversion harmonic processing [23]. In brief, when

127   two waves of equal amplitude but opposite phase propagate in a nonlinear material at a frequency f_0, the

128   linear component of the summed waves (spectral content at the fundamental frequency f_0) should vanish

129   while some of the nonlinear components (spectral content around the even harmonic frequencies, e.g.,

130    $2f_0$) should be doubled. This technique has been amply used to enhance the signal to noise ratio of

131   harmonic imaging in the medical field. The harmonic generation appears in the frequency band 150-

132   250kHz, above the sources bandwidth (150kHz) and below the signal to noise ratio (250kHz), depicted

133   with a blue background area in Figure 3b-1. The summed focused signal $(x_i^+ + x_i^-)$ are then filtered in

134   this frequency band (150-250 kHz). The residual intensity is reported to the strain amplitude in Figure

135 3b-2. We observe a quadratic evolution of this parameter with the strain amplitude. The retained value

136 for this nonlinear parameter is the quadratic term β of the fitted polynomial. The asymmetry of the

137 focused signals is representative of a difference between pushing and pulling at the surface. It is expected

138 to be sensitive to the crack interface through clapping phenomena [17].

139 The procedures are repeated for all 1600 points of the scanning grid to provide a map of the nonlinear

140 parameters. The linear and quadratic regression are calculated only for the 5 available strain amplitudes.

141 However, each point results from the combination of two independently ran signals. In addition, the

142 spatial measurement density (1.5 mm^2) in view of the mean wavelength (1 cm) allows the spatial

143 smoothing of the obtained images.

144

145   **3. Results and discussion**

146 The two images obtained using nonlinear ultrasound are displayed on Figure 4a and 4b respectively for

147 α and β parameters.

148 Fig. 4a reveals several zones surrounding the crack with a higher α parameter. In was shown in previous

149 work [16] that this parameter was related to the amount of micro-cracking damage in concrete. The size

150 of the micro-cracked region occurring before coalescence of connected microcracks is known to depend

151 on the size of the aggregates [18]. Our concrete sample being made with 22 mm aggregates, the size of

152 the fracture process zone is expected to scale about 2 cm apart from the crack [18,24]. This corresponds

153 to the extent of the highest α values shown in Fig 4b. This map of α seems to be a reasonable

154 representation of the fracture process zone [18,25,26].

155 In Figure 4b, the parameter β exhibits a relatively large dynamic range and is thus displayed in log scale

156 for clarity. The highest β values are observed along the crack lips and do not overlap with the map of

157 the α parameter. We explain the results as follow: some parts of the cracks can be opened and closed by

158 the push-pull induced by the ultrasonic focusing, generating the strong asymmetries in the signals, thus

159 producing a strong residual energy. As a correlation step, a vibro-thermography experiment is carried

160 out using the same sources at the same frequencies. One of the piezoelectric devices is driven at 400Vpp

161 (maximal amplitude reachable by the amplifiers), at the frequency which produces the highest amplitude

162 in the sample (80kHz). The images are recorded using a FLIR SC8200 IR camera. The image is obtained

163 using the protocol described by Remillieux et al. [27] to image cracks in metal. The image (Fig.4c)

164 reveals high intensity spots occurring during wave propagation in the crack region. The apparent

165 correlation of both images in Figures (4b,4c) suggests that both techniques are sensitive to the same

166 physical features of the crack despite the wavelength of the source signal being much larger than those

167 features.

168

169   **4. Conclusion**

170 This paper demonstrates the ability of nonlinear ultrasonic methods to image macrocrack processes in

171 concrete. The time reversal method employed here allows to image independently the fracture process

172 zone and the crack lips using two physical parameters (α and β) respectively sensitive to the presence of

173 diffused micro-damage and friction/clapping phenomena. The beta mapping is correlated with a vibro-

174 thermography image. The alpha mapping reveals a micro-damaged zone corresponding to the size of

175 already observed FPZ in samples with aggregate size of about 20mm.

176 In view of field applications, the method employed here presents the advantage that the location of the

177 sources is not an issue and it does not affect the resolution which is driven by the scan span defined with

178 the laser. However, the main limitation is the surface nature of the measurements even if the information

179 is also related to the penetration depth of the focal still driven by the wavelength. Another limitation of

180 the present experiment is the time needed to perform such a scan (about 80h) even if the spatial

181 resolution could be reduced to meet more realistic industrial conditions. Nonetheless, the main

182 conclusion concerns the ability of the two nonlinear ultrasonic parameters to image and characterize

183 fracture processes in concrete. From a more practical standpoint, recent technological advances using

184 ultrasonic phased arrays in concrete [28] could allow to image a macrocracks in the bulk of concrete

185 using nonlinear phenomenon similarly as nonlinear imaging methods employed in metals [29] in the

186 near future, once high amplitude waves will be available on such equipment.

187

190

191 **References**

192

193 [1] O. Büyüköztürk, Imaging of concrete structures, NDT & E Int. 31 (4) (1998) 233-243

194 [2] P. Rivard, G. Ballivy, C. Gravel, F. Saint-Pierre, Monitoring of an hydraulic structure affected by

195 ASR: A case study, Cem. Concr. Res. 40 (4) (2010) 676-680

196 [3] BS 1881: Part 203, Recommendations for measurement of the velocity of ultrasonic pulses in

197 concrete, London, 1986.

198 [4] A. Quiviger, C. Payan, J.F. Chaix, V. Ganier and J. Salin, Effect of the presence and size of a real

199 macro-crack on diffuse ultrasound in concrete, NDT & E Int. 45 (2012) 128-132.

200 [5] A. Quiviger, A. Girard, C. Payan, J.F. Chaix, V. Garnier, J. Salin, Influence of the depth and

201 morphology of real cracks on diffuse ultrasound in concrete: a simulation study, NDT & E Int. 60 (2013)

202 11-16.

203 [6] P. Antonaci, C.L.E. Bruno, A.S. Gliozzi, M. Scalerandi, Monitoring evolution of compressive

204 damage in concrete with linear and nonlinear ultrasonic methods, Cem. Concr. Res. 40 (7) (2010) 1106-

205 1113.

206 [7] J. Chen, A.R. Jayapalan, J.Y. Kim, K.E. Kurtis, L.J. Jacobs, Rapid evaluation of alkali–silica

207 reactivity of aggregates using a nonlinear resonance spectroscopy technique, Cem. Concr. Res. 40

208 (2010) 914-923.

209 [8] F. Bouchaala, C. Payan, V. Garnier and J.P. Balayssac, Carbonation Assessment in Concrete by

210 Nonlinear Ultrasound, Cem. Concr. Res. 41 (2011) 557–559.

211 [9] C. Payan, V. Garnier, J. Moysan, Effect of water saturation and porosity on the nonlinear elastic

212 response of concrete, Cem. Concr. Res. 40 (3) (2010) 473-476

213 [10] P. Antonaci, C.L.E. Bruno, P.G. Bocca, M. Scalerandi, A.S. Gliozzi, Nonlinear ultrasonic

214 evaluation of load effects on discontinuities in concrete, Cem. Concr. Res. 40 (2010) 340-346.

215 [11] J.-P. Zardan, C. Payan, V. Garnier and J. Salin, Effect of the presence and size of a localized

216 nonlinear source in concrete, J. Acoust. Soc. Am. 128(2010) EL38-EL42.

217 [12] H. Choi, G. Palacios, J.S. Popovics, and S.H. Chao, Monitoring Damage in Concrete Columns

218 Using Ultrasonic Tomography, ACI Struct. J. (2018) 545-558.

219 [13] E. Larose, A. Obermann, A. Digulescu, T. Planes, J.-F. Chaix, F. Mazerolle, G. Moreau, Locating

220 and characterizing a crack in concrete with diffuse ultrasound: A four-point bending test, J. Acoust. Soc.

221 Am. 138 (2015) 232-241.

222 [14] Y Zhang, E Larose, L Moreau, G d'Ozouville, Three-dimensional in-situ imaging of cracks in

223 concrete using diffuse ultrasound, Struct. Health Monit. 17 (2019) 279-284.

224 [15] Anderson, B.E., Remillieux, M.C., Le Bas, P.-Y. and Ulrich, T.J., 2019. Time reversal techniques.

225 In B. Kundu (Ed), Nonlinear Ultrasonic and Vibro-Acoustical Techniques for Nondestructive

226 Evaluation, 2019, pp. 547-581.

227 [16] C. Payan, T.J. Ulrich, P.Y. Le Bas, M. Griffa, P. Schuetz, M.C. Remillieux, T.A. Saleh, Probing

228 material nonlinearity at various depths by time reversal mirror, App. Phys. Lett. 104 (2014) 144102.

229 [17] T. J. Ulrich, P. A. Johnson, R.A. Guyer, Interaction Dynamics of Elastic Waves with a Complex

230 Nonlinear Scatterer through the Use of a Time Reversal Mirror, Phys. Rev. Lett. 98 (2007) 104301.

231 [18] K. Otsuka, H. Date, Fracture process zone in concrete tension specimen, Eng. Fract. Mech. 65

232 (2000) 111-131.

233 [19] B.E. Anderson, M. Griffa, C. Larmat, T.J. Ulrich, P.A. Johnson, Time reversal. Acoust. Today

234 4(1) (2008) 5–16

235 [20] M.C. Remillieux, B.E. Anderson, T.J. Ulrich, P.Y. Le Bas, C. Payan, Depth profile of a time-

236 reversal focus in an elastic solid, Ultrasonics 58 (2015) 60-66.

237 [21] Q.A. Vu, V Garnier, J.F. Chaix, C. Payan, M. Lott, J.N. Eiras, Concrete cover characterisation

238 using dynamic acousto-elastic testing and Rayleigh waves, Constr. Build. Mater. 114 (2016) 87-97.

239 [22] M. Lott, M.C. Remillieux, V Garnier, PY Le Bas, TJ Ulrich, C Payan, Nonlinear elasticity in rocks:

240 A comprehensive three-dimensional description, Phys. Rev. Mat. 1 (2) (2017), 023603.

241 [23] P.N. Burns, D. Hope Simpson, M.A. Averkiou, Nonlinear imaging, Ultrasound in Medicine and

242 Biology (26) (2000), S19 - S22

243 [24] S. Muralidhara, B.R. Prasad, H. Eskandari, B.L. Karihaloo, Fracture process zone size and true

244 fracture energy of concrete using acoustic emission, Constr. Build. Mater. 24(4) (2010), 479-486.

245 [25] D. Zhang, K. Wu, Fracture process zone of notched three-point-bending concrete beams, Cem.

246 Concr. Res. 29 (1999) 1887-1892.

247   [26] H. Mihashi, N. Nomura, S. Niiseki, Influence of aggregate size on fracture process zone of concrete

248   detected with three dimensional acoustic emission technique, Cem. Concr. Res. 21 (5) (1991) 737-744.

249   [27] M.C. Remillieux et al., Detecting and imaging stress corrosion cracking in stainless steel, with

250   application to inspecting storage canisters for spent nuclear fuel, NDT & E Int. 109 (2020) 102180.

251   [28] E. Niederleithinger, S. Maak, F. Mielentz, U.A. Effner, C. Strangfeld, J. Timofeev, Review of

252   recent developments in ultrasonic echo testing of concrete, 5th International Conference on Smart

253   Monitoring, Assessment and Rehabilitation of Civil Structures, August 2019 Potsdam, Germany (2019)

254   [29] Y. Ohara, H. Nakajima, S. Haupert, T. Tsuji, T. Mihara, Nonlinear ultrasonic phased array with

255   fixed-voltage fundamental wave amplitude difference for high-selectivity imaging of closed cracks, J.

256   Acoust. Soc. Am. 146 (2019) 266-277.

257   Figures
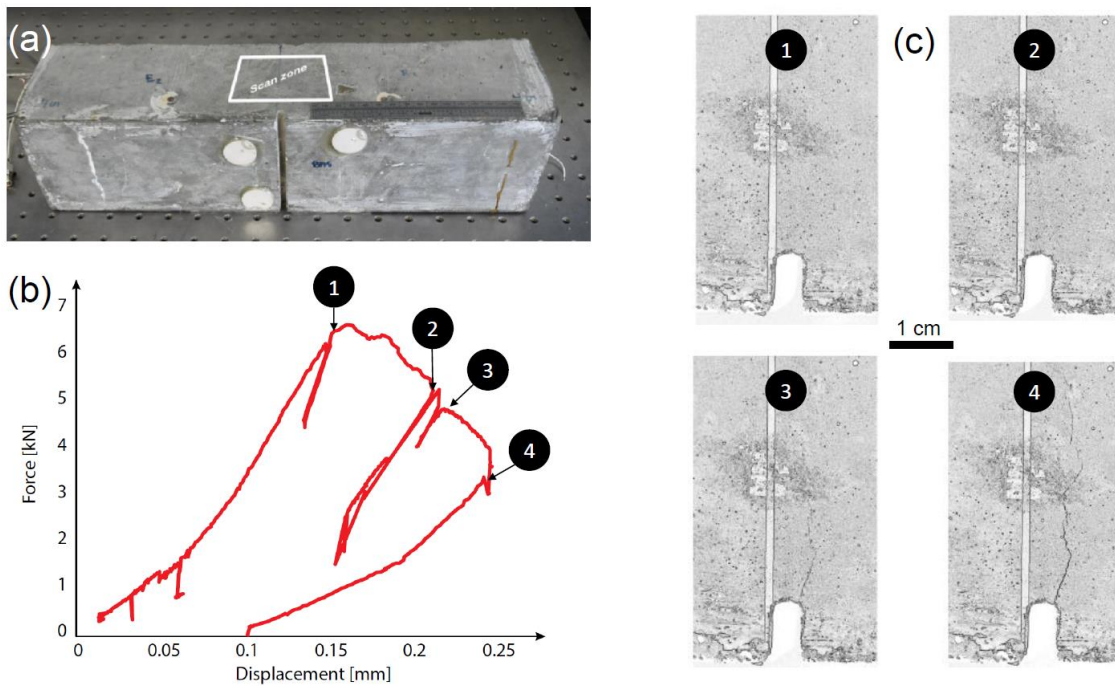
258

259   Figure 1. (a) Image of the sample showing where the acoustic scan zone is located. (b)

260   Force/displacement curved recorded during the mechanical test. 1 to 4 symbols represent the times when

261   the notched region was photographed. Corresponding images are shown in (c).
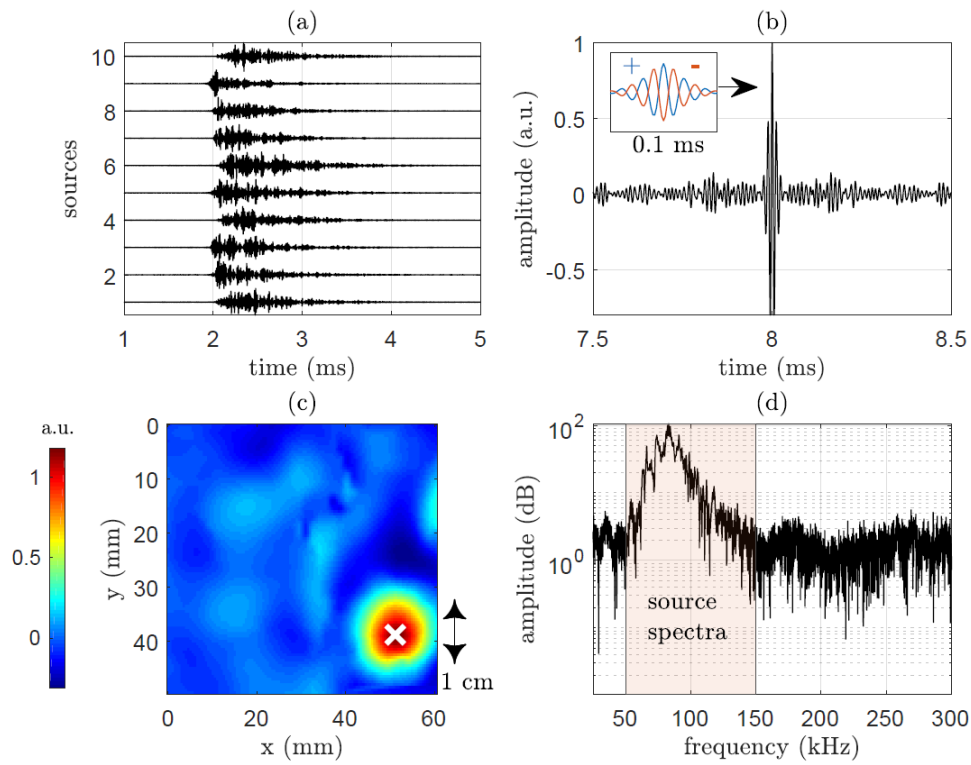
262

263

264

265

266

267

268

269

Figure 2: Time reversal mirror principle. (a) Ten forward signals sent by the sources. (b) Focused signal in time produced by rebroadcasting the time reversed version of the forward signals. (c) Focal spot in space (white-cross is the point where TRM is applied) recorded at focal time. (d) Frequency content of the focus signal. The input source spectra is highlighted by a red background area.

276
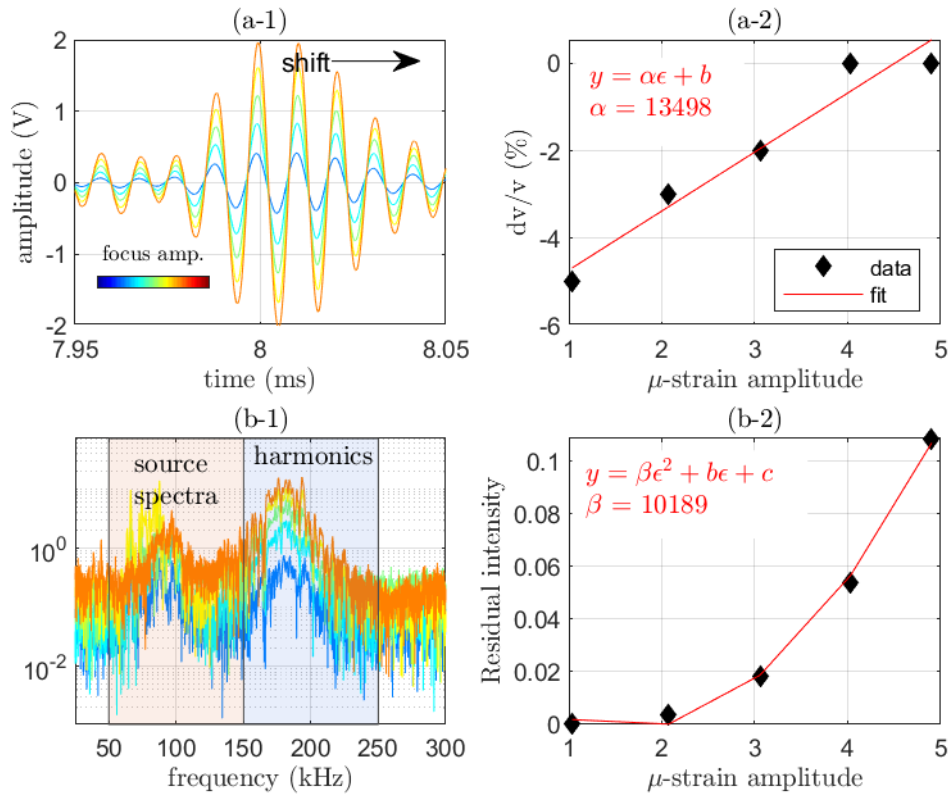
Figure 3: Representative results for the extraction of nonlinear parameters. (a) α and (b) β are extracted from the measured focused signal. (a-1) Five positive focused signals. (a-2) Time shift (or $\Delta t/t_0$) at the focal spot as a function of amplitude (black diamond) with a linear regression (red curve and equation). The color code (blue to red) represents the 5 focused amplitudes. (b-1) Residual spectra for the summation of the five positive and negative signals. The red background area is the linear frequency band (that of the source signal) and the blue background area is the frequency width considered for the harmonic generation measurement. (b-2) Residual intensity into the harmonic frequency band a function of strain amplitude (black diamond) and quadratic regression (red curve and equation).

289
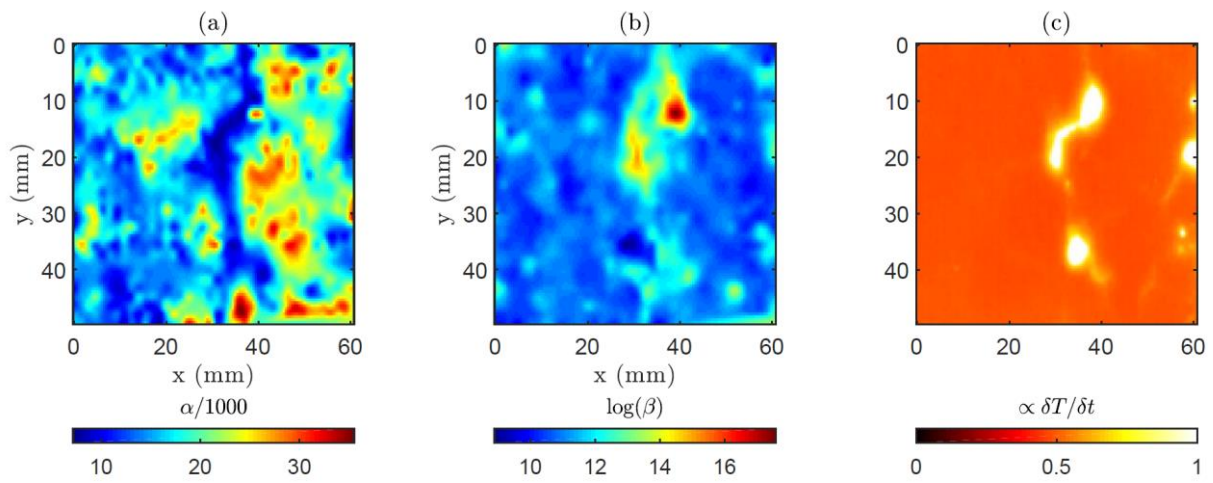
291 Figure 4: Experimental images of the cracked region. (a) Nonlinear α parameter. (b) Harmonic

292 generation (β parameter). (c) Vibro-thermography image: first derivative of the temperature with respect

293 to time (the reader can refer to [23] for more details).